Modification of electronic states of bcc Cr due to local atomic displacements around interstitial atoms B, C and N

1999 J. Phys.: Condens. Matter 11 767

(http://iopscience.iop.org/0953-8984/11/3/016)

J. Phys.: Condens. Matter **11** (1999) 767–778. Printed in the UK PII: S0953-8984(99)96997-7

Modification of electronic states of bcc Cr due to local atomic displacements around interstitial atoms B, C and N

Yoshihisa Matsumoto†§, Masahiko Morinaga† and Mitsuaki Furui‡

† Department of Materials Science and Engineering, Graduate School of Engineering, Nagoya University, Furo-cho, Chikusa-ku, Nagoya, Aichi 464-8603, Japan
‡ Department of System Engineering of Materials and Life Science, School of Engineering, Toyama University, Gofuku, Toyama 930-8555, Japan

Received 26 August 1998

Abstract. The electronic structures of metalloid elements, X (X = B, C, N) existing at the octahedral interstitial site in bcc Cr were calculated by the DV-X_α molecular orbital method. The covalent interaction between X and Cr atoms changed in the order B > C > N, whereas the ionic interaction changed in the reverse order. It was shown that the first-nearest-neighbour Cr atoms moved away from the metalloid element at the centre, by about 40% in the unit of half the lattice parameter. As a result, a nearly regular octahedron of Cr atoms was formed locally around the metalloid element. Such a calculated X–Cr distance in bcc Cr was found to be observed commonly in various crystal structures of Cr_mX_n compounds.

1. Introduction

When metalloid elements such as B, C and N occupy the octahedral interstitial sites in bcc chromium lattice, electronic structures are modified in the neighbourhood of these elements. In addition, local displacement of the neighbouring Cr atoms is expected to take place in the crystal lattice. Such a displacement problem has been treated in bcc Fe because of the metallurgical importance in the martensite phase in the Fe–C (or N) system [1–4]. From a series of experiments [1, 3, 5, 6] and calculations [4], it has been found that first-nearest-neighbour iron atoms from the central C (or N) atom are displaced greatly so that an approximately regular octahedron of iron atoms is formed around the C (or N) atom. However, no approach has been made to bcc Cr, because of experimental difficulties, since solubility limits of the metalloid elements such as B, C and N in Cr are as low as 100 appm at room temperature. Instead, it is known that a variety of Cr_mX_n (X = B, C, N) compounds appear in their binary Cr–X equilibrium phase diagrams [7].

In the present work, electronic structures of chromium containing B, C and N were calculated using the DV-X_α cluster method. The optimum distances between X and Cr atoms were estimated from the analysis of the chemical bond strengths between them. The results were compared with those of bcc Fe [4]. Furthermore, the estimated X–Cr distance in bcc Cr was also compared with the measured interatomic distance in various Cr_mX_n compounds.

§ On leave from Department of Computer and Control Engineering, Oita National College of Technology, Maki, Oita 870-0152, Japan.

0953-8984/99/030767+12$19.50

2. Computational method

The discrete variational (DV)-X_α method [8–11] is a molecular orbital calculation method assuming the Hartree–Fock–Slater approximation. In this method, the molecular orbitals are constructed by a linear combination of numerical atomic orbitals which are generated flexibly according to chemical environments. In this calculation, the parameter α is fixed at 0.7, an empirically appropriate value [10], and the self-consistent charge approximation is used. The matrix elements of the Hamiltonian and the overlap integrals are calculated by the weighted sum of integrant values at a large number of discrete sample points chosen randomly in real space, instead of employing a normal integration procedure. Therefore, no mathematical restriction is placed on the integration of these matrix elements. The atomic orbitals used in the present calculation were 1s–4p for Cr and 1s–2p for interstitial atoms, B, C and N.

For the characterization of the chemical bonding, the overlap population was calculated following the Mulliken population analysis [12]. The overlap population, $Q_{\nu\nu'}$, of electrons between two atoms ν and ν' is defined as

$$Q_{\nu\nu'} = \sum_k \sum_{i,j} C_{ik}^{\nu} C_{jk}^{\nu'} \int \Psi_i^{\nu} \Psi_j^{*\nu'} \, \mathrm{d}V. \tag{1}$$

Here, Ψ_i^{ν} and $\Psi_j^{\nu'}$ are the wavefunctions of the i and j orbitals of atoms ν and ν', respectively. C_{ik}^{ν} and $C_{jk}^{\nu'}$ are the coefficients which show the magnitude of the linear combination of atomic orbitals in the kth molecular orbital. The sum over k runs only over the occupied orbitals. Hereafter, $Q_{\nu\nu'}$ is called the bond order, Bo. This is a measure to show the covalent bond strength between atoms. In addition, the electron density of states was obtained from the energy level structure by using overlapping Gaussian function with the width of 0.2 eV and the centres located at each cluster energy level [13]. Also, electron density maps are used in order to observe directly the charge density distribution around an interstitial atom.

The model cluster employed in this calculation is shown in figure 1. This is a $Cr_{30}X$ (X = B, C or N) cluster with the D_{4h} symmetry. In this cluster only an X atom is located at the octahedral interstitial site in bcc Cr, because of a very limited solubility of X atoms in Cr, as described earlier. In the figure, $Cr^{(i)}$ means the ith-nearest-neighbour Cr atom from the central X atom in the cluster. As described earlier, the first-nearest-neighbour $Cr^{(1)}$ atoms may be displaced greatly in the direction away from the X atom, but the second-nearest-neighbour $Cr^{(2)}$ atoms may be displaced slightly because the X–$Cr^{(2)}$ distance is about 41% larger than the X–$Cr^{(1)}$ distance. Therefore, in the present calculation, only the $Cr^{(1)}$–$Cr^{(1)}$ distance, ℓ, was changed from $1.0\ell_0$ to $1.6\ell_0$ in the step of $0.1\ell_0$, where ℓ_0 is the $Cr^{(1)}$–$Cr^{(1)}$ distance in pure bcc Cr, 0.288 46 nm. Needless to say, ℓ_0 is equal to the lattice parameter of pure Cr. Moreover, for comparison the calculation was performed using a pure chromium cluster, Cr_{30}, which was made simply by removing a central X atom from the $Cr_{30}X$ cluster.

3. Results

3.1. Electron density of states

Some results for the electron density of states (DOS) are given in figure 2 for the pure Cr cluster (Cr_{30}) and the alloyed Cr clusters ($Cr_{30}B$, $Cr_{30}C$ and $Cr_{30}N$). For $Cr_{30}B$, the calculated results are presented in (b) for the non-displaced cluster ($\ell/\ell_0 = 1.0$) and in (c) for the displaced cluster ($\ell/\ell_0 = 1.4$). Here, ℓ/ℓ_0 was set to be 1.4 in the displaced cluster, because its value was most likely according to the bond order analysis as explained later. The DOS for pure Cr shown in (a) resembled the result of band calculations [14]. The Fermi energy level, E_F, lay

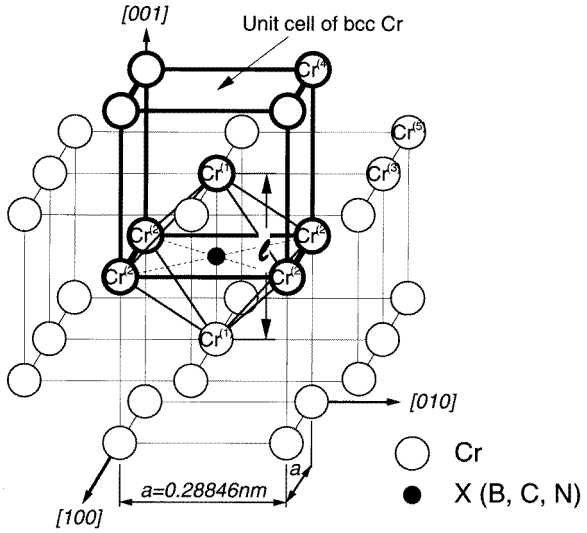

Figure 1. Cluster model, $Cr_{30}X$ (X = B, C, N) employed in the calculation. $Cr^{(1)}$, $Cr^{(2)}$, $Cr^{(3)}$, $Cr^{(4)}$ and $Cr^{(5)}$ denote the first-, second-, third-, fourth- and fifth-nearest-neighbour chromium atoms from an X atom at the octahedral interstitial site.

in the Cr 3d band. The DOS changed by the addition of an X atom into Cr, mainly due to the appearance of the X 2s and 2p components in it. So, in (b)–(e), the partial density of states (PDOS) for X 2s and 2p components is also shown in an enlarged scale ($\times 20$) together with the total DOS. By comparing figure 2(b) with (c), it was evident that as ℓ/ℓ_0 was varied from 1.0 to 1.4, attendant changes happened not only in the positions of main 2s and 2p peaks, but also in the distribution of other small peaks over a wide energy range. These modifications in the PDOS with ℓ/ℓ_0 will affect the interactions between B s, p and Cr d electrons, as explained later. This was also the case for C and N. In addition, since the Cr 3d band lay closer to the energy region of the X 2p component than that of the X 2s component, the p–d interaction was supposed to be stronger than the s–d interaction in these alloyed Cr. Furthermore, the positions of main X 2s and 2p peaks changed systematically with the atomic number of the metalloid elements, X. Namely, they were deeper in $Cr_{30}N$ than in $Cr_{30}C$ than in $Cr_{30}B$. This implies that the covalent interaction between Cr and X atoms changes in the order Cr–B > Cr–C > Cr–N, as described later.

3.2. Bond order changes with interstitial atoms

Both the Cr-Cr and the X–Cr bond orders were calculated by changing the ℓ/ℓ_0 value in the range of 1.0 to 1.6. The results are shown in figure 3(a) for the total Cr–Cr bond order between Cr s, p, d and Cr s, p, d electrons, and (b) for the total X–Cr bond order between X s, p and Cr s, p, d electrons. The Cr–Cr bond order gradually increased until the ℓ/ℓ_0 value reached 1.3–1.4 regardless of X, and then it was saturated. This saturated value was close to the total Cr–Cr bond order for pure Cr calculated by using a Cr_{30} cluster. Thus, the Cr–Cr bond order decreased by introducing an X atom into Cr without any atomic displacements, but it was recovered to the original value of pure Cr by the displacements of the $Cr^{(1)}$ atoms. On the other hand, the X–Cr bond order shown in (b) increased abruptly with ℓ/ℓ_0, and then it reached a plateau near 1.4 for the ℓ/ℓ_0 value, nearly independent of X atoms. In the case of B, the plateau may occur

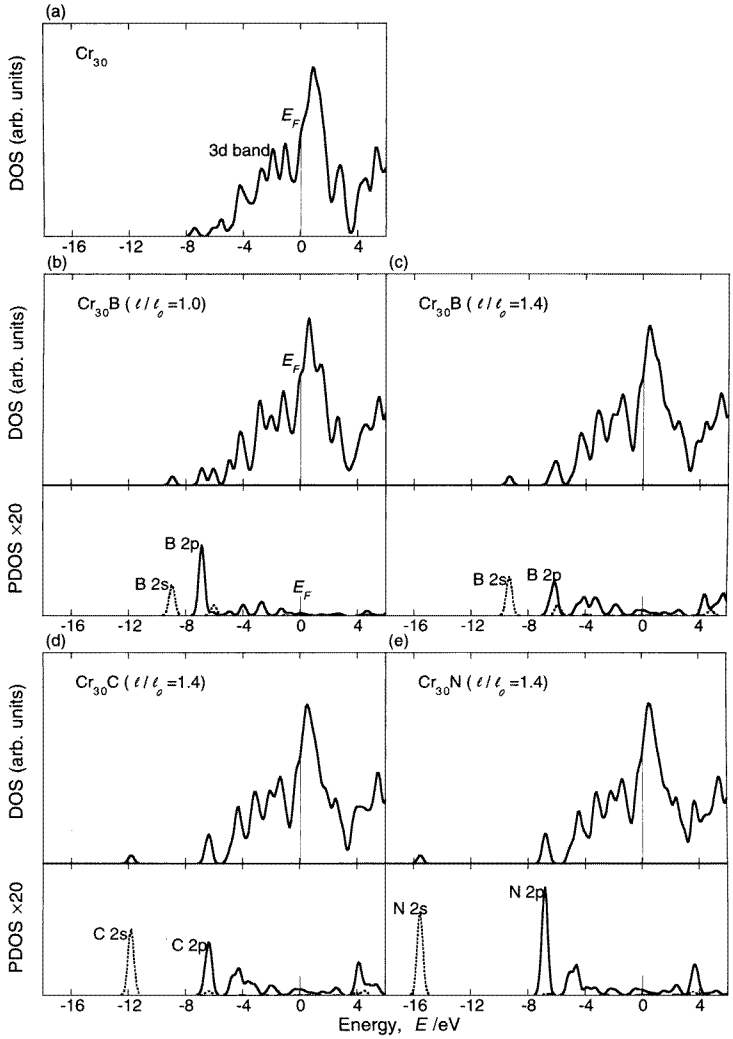

Figure 2. Total and partial electron densities of states for (a) Cr_{30}, (b) $Cr_{30}B$, $\ell/\ell_0 = 1.0$, (c) $Cr_{30}B$, $\ell/\ell_0 = 1.4$, (d) $Cr_{30}C$, $\ell/\ell_0 = 1.4$ and (e) $Cr_{30}N$, $\ell/\ell_0 = 1.4$.

at a position slightly larger than 1.4, probably due to the larger atomic radius of B than C or N. But the deviation was supposed to be still small. The magnitude of the X–Cr bond order at the plateau changed in the order B > C > N, indicating that the covalent interaction between X and Cr atoms changed following this order, as described earlier.

3.3. Components of X–Cr bond orders

The components of the X–Cr bond order were further examined in detail. Figure 4(a), (b) and (c) shows the results of the B–Cr, the C–Cr and the N–Cr bond order, respectively. Every bond order shown in this figure is the value per bond.

Any X–$Cr^{(3)}$, X–$Cr^{(4)}$ and X–$Cr^{(5)}$ bond orders were nearly nil, regardless of X atoms, because of the long interatomic distances between them. On the other hand, both the X–$Cr^{(1)}$

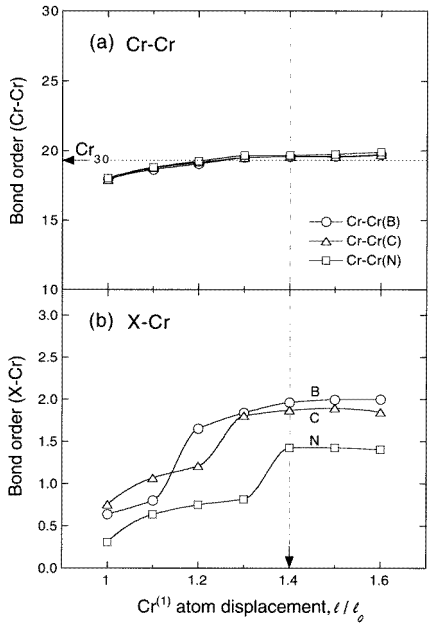

Figure 3. Changes of (a) Cr–Cr bond order and (b) X–Cr bond order with the $Cr^{(1)}$ atomic displacement, ℓ/ℓ_0.

and X–$Cr^{(2)}$ bond orders were much larger and changed significantly with ℓ/ℓ_0. For example, the X–$Cr^{(2)}$ bond order, shown by open circles in each figure, increased monotonically with increasing ℓ/ℓ_0. On the other hand, the X–$Cr^{(1)}$ bond order shown by closed circles was very small when $\ell/\ell_0 = 1.0$, but it increased continuously with ℓ/ℓ_0 and showed a broad peak near 1.3 for ℓ/ℓ_0, followed by a gradual decrease with ℓ/ℓ_0.

For comparison, the results of C interstitials in bcc Fe are shown in figure 4(d) [4], although the cluster model used for the calculation was $Fe_{14}C$, smaller than the present one, $Cr_{30}C$. When comparing the C–Fe bond order shown in (d) with the C–Cr bond order shown in (b), it was apparent that the C–$Fe^{(2)}$ bond order curve was similar to the C–$Cr^{(2)}$ bond order curve, whereas the C–$Fe^{(1)}$ bond order curve was very different from the C–$Cr^{(1)}$ bond order curve. This difference was not attributable to the difference in the cluster models between two calculations, because nearly the same C–$Cr^{(1)}$ bond order curve was obtained even from the calculation using a small $Cr_{14}C$ cluster, the same size cluster as $Fe_{14}C$. The very small value of the C–$Cr^{(1)}$ bond order in the non-displaced cluster (i.e., $\ell/\ell_0 = 1.0$), implied that the C–$Cr^{(1)}$ interatomic distance (0.1442 nm) was too short to make a stable chemical bond between them. As was evident from the C–$Cr^{(1)}$ bond order change with ℓ/ℓ_0, the increasing interatomic distance could strengthen the chemical bond between them. But this is no longer true for bcc Fe, since the C–$Fe^{(1)}$ interatomic distance (0.1435 nm) may be long enough to make a stable chemical bond between them, because of the smaller atomic size of Fe than Cr. So, the increasing C–$Fe^{(1)}$ distance will weaken the chemical bond between them, which is in contrast to the result of the C–$Cr^{(1)}$ bond order.

Table 1 shows the respective values of the components in the X–$Cr^{(1)}$ and the X–$Cr^{(2)}$ bond orders. It was apparent that the X 2p–Cr 3d component was largest among the components of both the X–$Cr^{(1)}$ and the X–$Cr^{(2)}$ bond orders. However, this 2p–3d component decreased

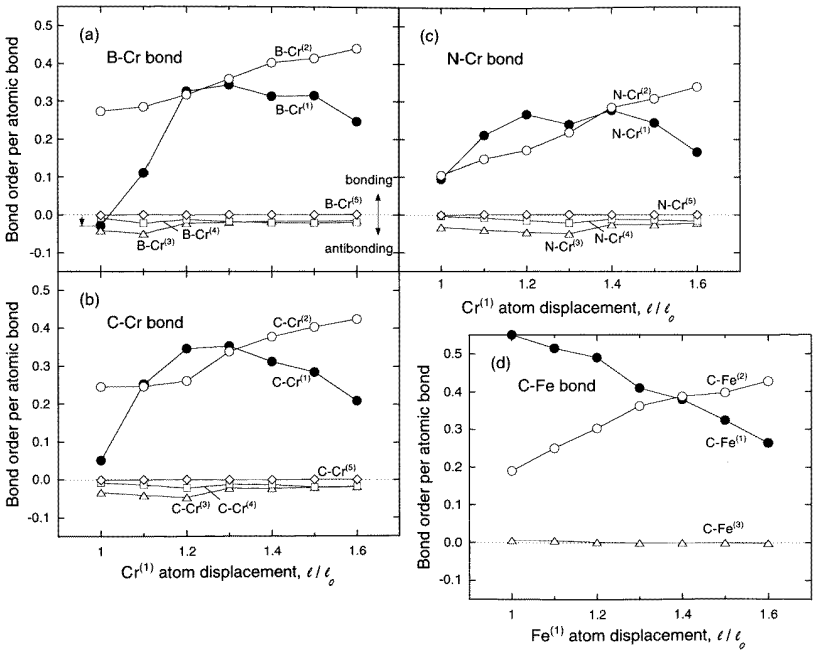

Figure 4. Changes of the components in the X–Cr bond order with the $Cr^{(1)}$ atomic displacement, ℓ/ℓ_0, for (a) B–Cr bond, (b) C–Cr bond and (c) N–Cr bond. Also, in (d) the components in the C–Fe bond order was reproduced from [4].

with increasing ℓ/ℓ_0 in case of the X–$Cr^{(1)}$ bond order, but increased in case of the X–$Cr^{(2)}$ bond order. A similar change was also seen in the X 2s–Cr 3d component. As a result, the magnitudes of these components became similar between the X–$Cr^{(1)}$ and X–$Cr^{(2)}$ bond orders when $\ell/\ell_0 = 1.4$. Also, most of the components in the X–$Cr^{(2)}$ bond order increased with ℓ/ℓ_0, and approached the values of the corresponding components in the X–$Cr^{(1)}$ bond order.

3.4. Difference electron density maps

The spatial electron distribution in the cluster was examined using the difference electron density, $\Delta\rho$, between the non-displaced cluster and the displaced cluster. The calculated difference electron density maps on the (110) atomic plane are shown in figure 5. The difference electron densities shown in (a) and (b) are defined as

$$\Delta\rho_1 = \rho[Cr_{30}C(\ell/\ell_0 = 1.0)] - \rho[Cr_{30}(\ell/\ell_0 = 1.0)] \tag{2}$$

and

$$\Delta\rho_{1.4} = \rho[Cr_{30}C(\ell/\ell_0 = 1.4)] - \rho[Cr_{30}(\ell/\ell_0 = 1.4)] \tag{3}$$

respectively. Here, $\rho[Cr_{30}C(\ell/\ell_0 = 1.0 \text{ or } 1.4)]$ and $\rho[Cr_{30}(\ell/\ell_0 = 1.0 \text{ or } 1.4)]$ are the electron densities in the corresponding cluster shown in the parenthesis. Therefore, $\Delta\rho_1$ and $\Delta\rho_{1.4}$ describe the changes in the charge density arising from the introduction of a carbon atom into the non-displaced and the displaced clusters, respectively. The region where $\Delta\rho > 0$ is indicated by full curves and the region where $\Delta\rho \leqslant 0$ is indicated by broken curves. Namely, there are excess electrons in the region where $\Delta\rho > 0$, and deficient electrons in the region where $\Delta\rho \leqslant 0$.

Table 1. Components of the X–Cr bond order in the $Cr_{30}X$ cluster (X = B, C, N); (a) X–$Cr^{(1)}$ and (b) X–$Cr^{(2)}$.

		X 2s–Cr			X 2p–Cr		
	ℓ/ℓ_0	2s–3d	2s–4s	2s–4p	2p–3d	2p–4s	2p–4p
(a) X–$Cr^{(1)}$							
$Cr_{30}B$	1.0	0.152	−0.065	−0.016	0.451	−0.146	0.044
	1.4	0.062	0.012	0.042	0.146	0.031	0.088
$Cr_{30}C$	1.0	0.180	−0.070	−0.027	0.466	−0.088	0.058
	1.4	0.051	0.004	0.041	0.151	0.045	0.085
$Cr_{30}N$	1.0	0.174	−0.056	0.021	0.432	−0.064	0.061
	1.4	0.036	−0.004	0.036	0.125	0.050	0.093
(b) X–$Cr^{(2)}$							
$Cr_{30}B$	1.0	0.047	0.033	0.051	0.105	0.045	0.065
	1.4	0.056	0.035	0.056	0.184	0.069	0.073
$Cr_{30}C$	1.0	0.037	0.026	0.051	0.101	0.032	0.060
	1.4	0.051	0.020	0.050	0.168	0.062	0.084
$Cr_{30}N$	1.0	0.015	0.002	0.014	0.086	0.010	0.040
	1.4	0.037	0.003	0.029	0.143	0.052	0.075

In $\Delta\rho_1$ shown in (a), positive contour lines around a carbon site are nearly elliptical with the major axis lying along the C–$Cr^{(1)}$ direction, and also positive contour lines are extended over the $Cr^{(2)}$ atoms. However, as shown in (b), once the local displacement was introduced into the crystal (i.e., $\ell/\ell_0 = 1.4$), the electron density distribution changed nearly spherically, as might be expected from the cubic symmetry of the interstitial site in a regular octahedron when $\ell/\ell_0 = 1.4$. When comparing (b) with (a), it is apparent that both the covalency between C and $Cr^{(1)}$ and between C and $Cr^{(2)}$ increases with this displacement, in agreement with the results of bond order calculations shown in figure 4(b).

For comparison, the results of C interstitials in bcc Fe are also shown in (c) and (d) [4], although the cluster model used for the calculation was $Fe_{14}C$, as explained before. When comparing the $\Delta\rho_1(Fe_{14}C)$ shown in (c) with the $\Delta\rho_1(Cr_{30}C)$ shown in (a), it was apparent that the electron density distribution in the C–$Fe^{(2)}$ direction resembled that in the C–$Cr^{(2)}$ direction. However, a higher electron density region around a carbon site was extended over the neighbouring $Fe^{(1)}$ atom site in the $\Delta\rho_1(Fe_{14}C)$, but it was less extended in the $\Delta\rho_1(Cr_{30}C)$. This implied that for $Fe_{14}C$ there was stronger covalent bonding between C and $Fe^{(1)}$ atoms than between C and $Fe^{(2)}$ atoms. On the other hand, as shown in (d), when $\ell/\ell_0 = 1.4$, the appearance of the spherical electron density distribution in $\Delta\rho_{1.4}(Fe_{14}C)$ was similar to that in $\Delta\rho_{1.4}(Cr_{30}C)$.

3.5. Orbital populations and net charge of atoms

The orbital populations of valence electrons occupying each orbital were evaluated following the Mulliken population analysis, and the results are listed in table 2. The orbital populations were modified by the displacement of $Cr^{(1)}$ atoms. For example, for the $Cr_{30}B$ cluster, in the non-displaced case, (i.e., $\ell/\ell_0 = 1.0$), the population of the $Cr^{(1)}$ 3d electrons was larger than that of pure Cr (i.e., Cr_{30}), but instead the populations of $Cr^{(1)}$ 4s and 4p electrons were smaller. However, once the local displacement was introduced into the crystal (i.e., $\ell/\ell_0 = 1.4$), the population of the $Cr^{(1)}$ 3d electrons decreased, whereas the populations of 4s and 4p electrons increased. As a result each orbital population of the $Cr^{(1)}$ atom approached the values of

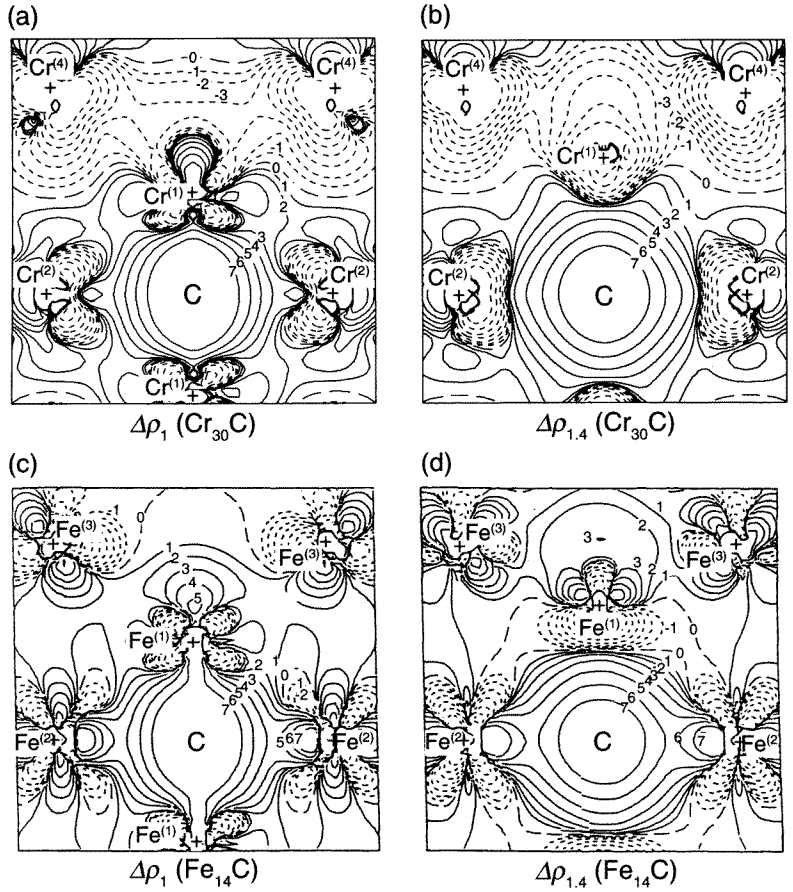

Figure 5. The difference electron density maps on the (110) atomic plane for (a) $\Delta\rho_1$ ($Cr_{30}C$) and (b) $\Delta\rho_{1.4}$ ($Cr_{30}C$). Also, in (c) and (d) the $\Delta\rho_1$ and $\Delta\rho_{1.4}$ for $Fe_{14}C$ were reproduced from [4] . The curve labels, 0, ±1, ±2, ±3, ±4, ±5, ±6, ±7, correspond to the values of electron density, 0, ±0.002, ±0.004, ±0.008, ±0.016, ±0.032, ±0.064, ±0.128, respectively, in electrons per atomic unit cubed.

the $Cr^{(1)}$ atom in pure Cr. In other words, the electronic state of the $Cr^{(1)}$ atom recovered to some extent when it was displaced. This was also the case for C and N. A similar but weaker tendency was seen in the 3d and 4s orbital populations of the $Cr^{(2)}$ atom, regardless of X (B, C, N) atoms.

These results will be associated partially with the decrease in the X s, p–$Cr^{(1)}$ d bond order and with the increase in the X s, p–$Cr^{(1)}$ s, p bond order with ℓ/ℓ_0 as explained before. For example in the case of B, the decrease in the population of $Cr^{(1)}$ 3d electrons was attributable to the weakening of the B s, p-$Cr^{(1)}$ d bond, whereas the increase in the populations of $Cr^{(1)}$ 4s and 4p electrons were attributable to the strengthening of the B s, p-$Cr^{(1)}$ s, p bond. In addition, as shown in table 2, the population of B 2s electrons increased with ℓ/ℓ_0, whereas the population of B 2p electrons decreased. The spherical s-type orbital may be preferable to the directional p-type orbital, since the bonding between B and Cr becomes nearly isotropic when $\ell/\ell_0 = 1.4$. This was also true in other interstitials, C and N.

Table 2. Orbital populations of valence electrons in $Cr^{(i)}$ and X atoms and net charges of X atoms in Cr_{30} and $Cr_{30}X$ (X = B, C, N) clusters.

		Cr_{30}	$Cr_{30}B$		$Cr_{30}C$		$Cr_{30}N$	
		$\ell/\ell_0 = 1.0$	$\ell/\ell_0 = 1.0$	$\ell/\ell_0 = 1.4$	$\ell/\ell_0 = 1.0$	$\ell/\ell_0 = 1.4$	$\ell/\ell_0 = 1.0$	$\ell/\ell_0 = 1.4$
$Cr^{(1)}$	3d	4.506	4.767	4.575	4.747	4.557	4.697	4.539
	4s	0.586	0.494	0.513	0.464	0.521	0.484	0.536
	4p	1.041	0.916	1.018	0.880	1.003	0.898	0.995
$Cr^{(2)}$	3d	4.377	4.403	4.389	4.405	4.386	4.423	4.389
	4s	0.629	0.550	0.575	0.536	0.562	0.528	0.556
	4p	0.925	0.982	0.989	0.963	0.976	0.933	0.948
$Cr^{(3)}$	3d	4.548	4.517	4.505	4.512	4.507	4.519	4.512
	4s	0.642	0.643	0.645	0.643	0.646	0.646	0.647
	4p	0.577	0.629	0.645	0.642	0.648	0.636	0.645
$Cr^{4)}$	3d	4.488	4.485	4.539	4.488	4.533	4.484	4.534
	4s	0.663	0.661	0.648	0.660	0.647	0.662	0.645
	4p	0.659	0.637	0.595	0.643	0.602	0.648	0.605
$Cr^{(5)}$	3d	5.095	5.089	5.090	5.090	5.091	5.089	5.091
	4s	0.950	0.918	0.876	0.912	0.872	0.907	0.872
	4p	0.495	0.528	0.576	0.533	0.582	0.537	0.584
X (B, C or N)	2s		0.822	0.990	1.346	1.371	1.606	1.659
	2p		2.347	2.199	3.015	2.938	3.776	3.742
Net charge of X			−0.173	−0.190	−0.363	−0.311	−0.383	−0.402

The net charge of the X atom was negative as shown in table 2, indicating that charge transfer occurred from Cr to X atoms in these systems. Among B, C and N, the net charge changed in the order B > C > N. Therefore, the ionic interaction due to the charge transfer between atoms changed in the reverse order, B < C < N, in agreement with the order of the electronegativity of these metalloid elements.

4. Discussion

4.1. Interatomic distances in chromium compounds

It may be expected that the calculated X–Cr interatomic distances in bcc Cr are reflected in the interatomic distances even in a variety of Cr_mX_n compounds [15, 16]. In figure 6(a)–(c), the bond orders between X and $Cr^{(i)}$ atoms in bcc Cr are plotted against the radial distances between them. For example, in the figure, the arrow of $Cr^{(i)}$ put on the horizontal axis shows, the location of $Cr^{(i)}$ atom, being distant from the X atom at the centre. Also, $Cr^{(1)}$ and $Cr^{(1)'}$ denote the location of the $Cr^{(1)}$ atom in the non-displaced cluster (i.e., $\ell/\ell_0 = 1.0$) and in the displaced cluster (i.e., $\ell/\ell_0 = 1.4$), respectively. Needless to say, the $Cr^{(1)'}$ location is close to the $Cr^{(2)}$ location, since the X–$Cr^{(1)}$ distance becomes nearly equal to the X–$Cr^{(2)}$ distance when $\ell/\ell_0 = 1.4$. In addition, the bond order curves were distinguished between the non-displaced and the displaced clusters by using dotted and solid lines in the figure respectively. Also, in figure 6(a′)–(c′), experimental values of the shortest X–Cr and X–X interatomic distances [15] are shown for various Cr_mX_n compounds.

It was apparent that the shortest X–Cr interatomic distance was close to the X–$Cr^{(1)'}$ (or $Cr^{(2)}$) distance, nearly independent of X atoms. Only in the case of B, the shortest B–Cr interatomic distance may be slightly longer than the expected distance from bcc Cr with 1.4 for ℓ/ℓ_0. But this also may be understood from the bond order curve shown in figure 3(b), since

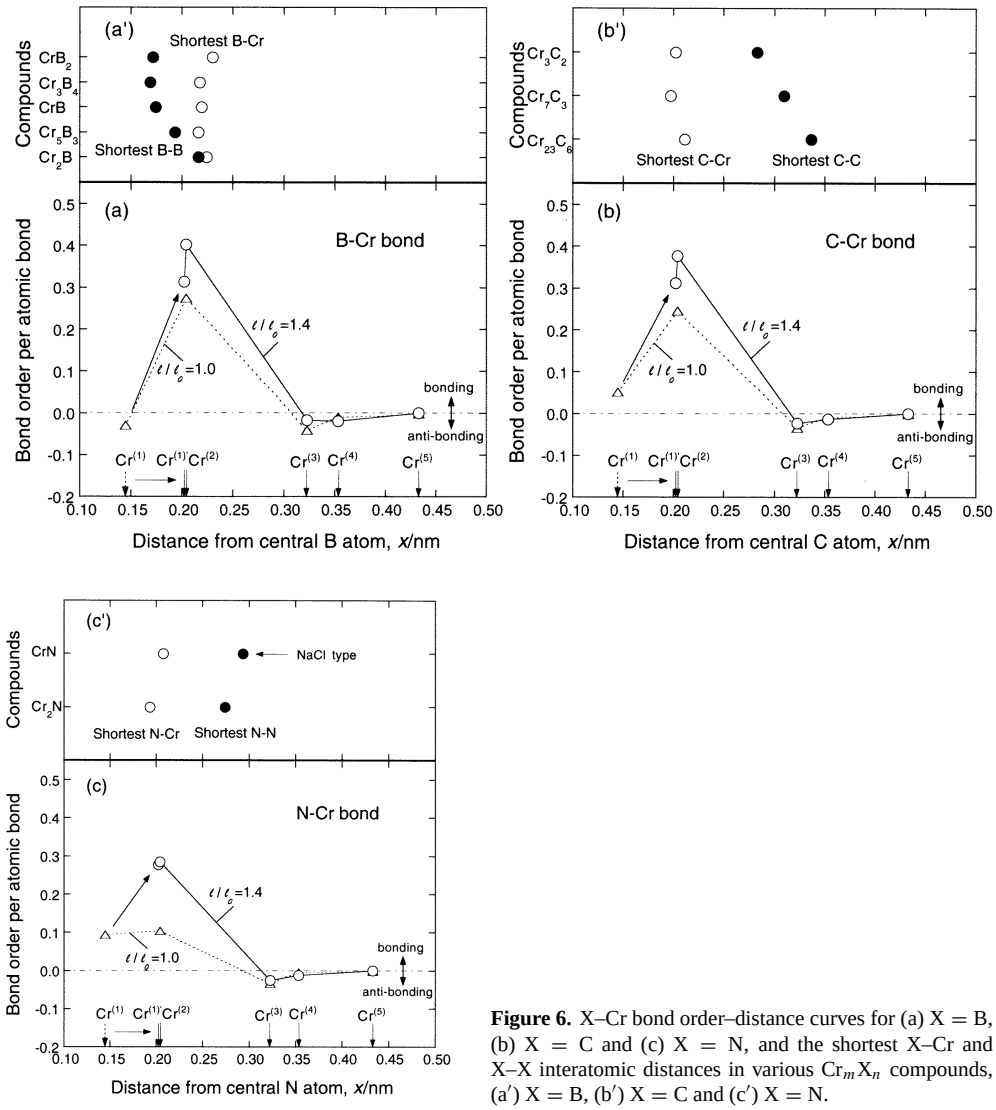

Figure 6. X–Cr bond order–distance curves for (a) X = B, (b) X = C and (c) X = N, and the shortest X–Cr and X–X interatomic distances in various Cr_mX_n compounds, (a′) X = B, (b′) X = C and (c′) X = N.

the ℓ/ℓ_0 value at the plateau may be slightly larger than 1.4, as explained earlier. Thus, the interatomic distance obtained from the present calculation of bcc Cr was indeed reflected in the interatomic distance in their compounds. On the other hand, the shortest X–X interatomic distance fell approximately on the $Cr^{(3)}$ location in the horizontal axis, except for X = B. Recalling that the X–Cr bond order became nil at this $Cr^{(3)}$ location, we may suppose that C (or N) atoms are located in these compounds as if the C (or N)–Cr interactions are not disturbed by the existence of another C (or N) atom in the neighbourhood. In other words, it seems that the C (or N)–Cr interactions are dominant, but the C–C (or N–N) interactions are of little importance in the chromium carbides (or nitrides). However, this explanation is no longer valid for chromium borides since the B–B distance is much shorter than the B–Cr distance. This clearly indicates that the B–B interaction is important in addition to the B–Cr interaction in the chromium borides, as reported in previous band calculations [17–19].

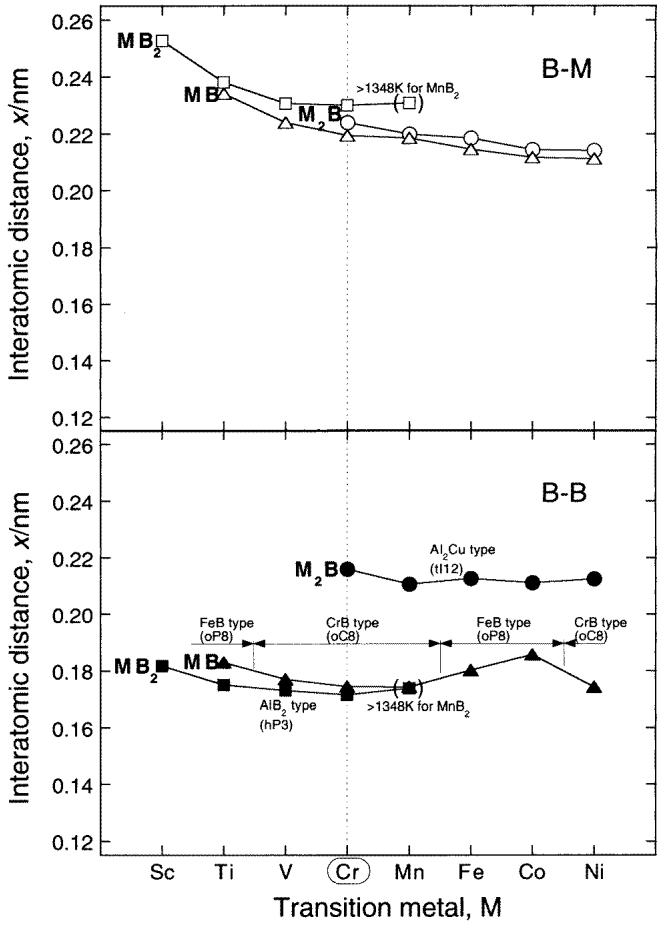

Figure 7. Comparison of the B–M and B–B interatomic distances among a variety of the 3d transition-metal borides, M_2B, MB and MB_2.

4.2. Interatomic distances in 3d transition-metal borides

Further examination of the interatomic distances was carried out by comparing them among the 3d transition-metal semiborides (M_2B), monoborides (MB) and diborides (MB_2) [15]. Figure 7 shows the shortest B–M and B–B interatomic distances in them, where M are 3d transition metals. In all the cases, the B–B interatomic distances are shorter than the B–M interatomic distance, regardless of M. The B–M interatomic distances in any borides decrease monotonically with the increase in the atomic number of M. This is reasonable since the atomic radius of M changes in this order. On the other hand, the B–B interatomic distance is nearly independent of M in each boride system (e.g., M_2B). It varies in the order $M_2B > MB > MB_2$. As might be expected, the lower B concentration in the compound makes the B–B interatomic distance longer. These characteristics of the B–B interatomic distance imply that the B–B interaction is significantly large in these borides and it is scarcely affected by the presence of M metals in them. This is true in any M metals including Cr. In contrast, as explained before, for chromium carbides and nitrides, the C–C (or N–N) interaction is of less importance, compared

to the C–Cr (or N–Cr) interaction. In this sense, it may be said that the borides are very different from the carbides and the nitrides in the nature of the chemical bond between atoms.

5. Conclusions

The electronic structures of bcc Cr containing interstitial atoms X (X = B, C, N) were calculated by the DV-X_α cluster method. The covalent interaction between X and Cr atoms changed in the order B > C > N, and the ionic interaction due to the charge transfer between them changed in the reverse order. It was found that the first-nearest-neighbour Cr atoms were displaced in the direction away from an X atom at the centre. As a result a nearly regular octahedron around the interstitial X atom was formed in the bcc Cr lattice. The distance between X and the first-nearest-neighbour Cr atoms was about 1.4 times longer than the original distance in the bcc lattice, nearly independent of X atoms. Such an X–Cr interatomic distance estimated in bcc Cr was also seen in a variety of Cr_mX_n compounds, and hence similar atomic interactions seemed to be operating between Cr and X atoms even in the compounds.

Acknowledgments

The authors would like to acknowledge the staff of Computer Center of the Institute for Molecular Science, Okazaki National Institutes for the use of the NEC SX-3, model 34R supercomputer. This research was supported in part by the Grant-in-Aid for Scientific Research from the Ministry of Education, Science, Sports and Culture of Japan.

References

[1] Cochardt A W, Schoek G and Wiedersich H 1955 *Acta Metall.* **3** 533
[2] Moss S C 1967 *Acta Metall.* **15** 1815
[3] Cheng L, Böttger A, Keijser T H and Mittemeijer E J 1990 *Scr. Metall.* **24** 509
[4] Morinaga M, Yukawa N, Adachi H and Mura T 1987 *J. Phys. F: Met. Phys.* **17** 2147
[5] Williamson G K and Smallmann R E 1953 *Acta Crystallogr.* **6** 361
[6] He B, Rao S and Houska C R 1990 *J. Mater. Sci.* **25** 2667
[7] Massalski T B (ed) 1990 *Binary Phase Diagrams* 2nd edn, vols 1–3 (Metals Park, OH: American Society for Metals)
[8] Slater J C 1979 *The Calculation of Molecular Orbitals* (New York: Wiley)
[9] Averill F W and Ellis D E 1973 *J. Chem Phys.* **59** 6413
[10] Adachi H, Tsukada M and Satoko C 1978 *J. Phys. Soc. Japan* **45** 875
[11] Adachi H and Imoto S 1978 *Bull. Japan Inst. Met.* **17** 490
Adachi H and Imoto S 1978 *Bull. Japan Inst. Met.* **17** 495
[12] Mulliken R S 1955 *J, Chem. Phys.* **23** 1833
Mulliken R S 1955 *J, Chem. Phys.* **23** 1841
Mulliken R S 1955 *J, Chem. Phys.* **23** 2338
Mulliken R S 1955 *J, Chem. Phys.* **23** 2343
[13] Satoko C, Tsukada M and Adachi H 1978 *J. Phys. Soc. Japan* **45** 1333
[14] Fu C L and Freeman A J 1986 *Phys. Rev.* B **33** 1755
[15] Villars P and Calvert L D (ed) 1985 *Pearson's Handbook of Crystallographic Data for Intermetallic Phases* vols 1–3 (Metals Park, OH: American Society for Metals)
[16] Wyckoff R W G 1963 *Crystal Structures* 2nd edn, vols 1 and 2 (New York: Wiley)
[17] Mohn P and Pettifor D G 1988 *J. Phys. C: Solid State Phys.* **21** 2829
[18] Mohn P 1988 *J. Phys. C: Solid State Phys.* **21** 2841
[19] Guillermet A F and Grimvall G 1991 *J. Less-Common Met.* **169** 257